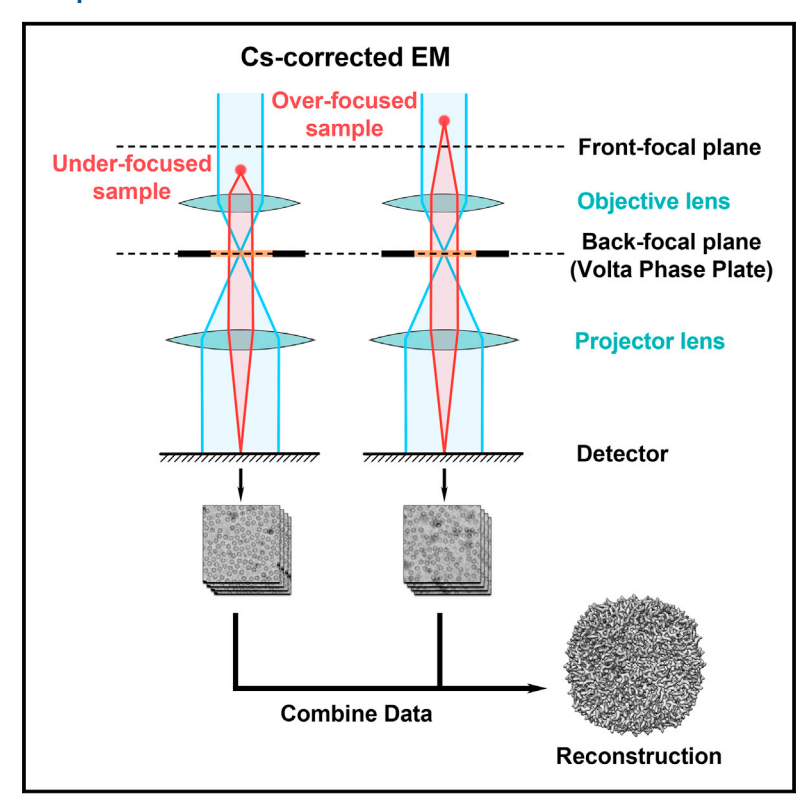
# **Structure**

# **Near-Atomic Resolution Structure Determination in Over-Focus with Volta Phase Plate by Cs-Corrected** Cryo-EM

# **Graphical Abstract**



# **Authors**

Xiao Fan, Lingyun Zhao, Chuan Liu, ..., Hai-Lin Peng, Jianlin Lei, Hong-Wei Wang

# Correspondence

jllei@tsinghua.edu.cn (J.L.), hongweiwang@tsinghua.edu.cn (H.-W.W.)

#### In Brief

Fan et al. took a unique advantage of the optical system by combining the Volta phase plate and Cs-corrector in a modern TEM to collect high-resolution micrographs of frozen-hydrated apoferritin in over-focus imaging conditions and determine the structure of apoferritin at 3.0 Å resolution.

# **Highlights**

- Successful combination of phase plate and Cs-corrector in single-particle cryo-EM
- Near-atomic structure determined from over-focused images by cryo-EM
- VPP-Cs-corrector coupled EM provides interesting optical properties





# Near-Atomic Resolution Structure Determination in Over-Focus with Volta Phase Plate by Cs-Corrected Cryo-EM

Xiao Fan,<sup>1,2,7</sup> Lingyun Zhao,<sup>1,2,7</sup> Chuan Liu,<sup>1,2</sup> Jin-Can Zhang,<sup>3,4</sup> Kelong Fan,<sup>5</sup> Xiyun Yan,<sup>5,6</sup> Hai-Lin Peng,<sup>3,4</sup> Jianlin Lei,<sup>1,\*</sup> and Hong-Wei Wang<sup>1,2,8,\*</sup>

<sup>1</sup>Ministry of Education Key Laboratory of Protein Sciences, Beijing Advanced Innovation Center for Structural Biology, School of Life Sciences, Tsinghua University, Beijing 100084, China

<sup>2</sup>Tsinghua-Peking Joint Center for Life Sciences, Tsinghua University, Beijing 100084, China

<sup>3</sup>Center for Nanochemistry, Beijing Science and Engineering Center for Nanocarbons, Beijing National Laboratory for Molecular Sciences, College of Chemistry and Molecular Engineering, Peking University, Beijing 100871, China

<sup>4</sup>Academy for Advanced Interdisciplinary Studies, Peking University, Beijing 100871, China

<sup>5</sup>Key Laboratory of Protein and Peptide Pharmaceuticals, CAS-University of Tokyo Joint Laboratory of Structural Virology and Immunology, Institute of Biophysics, Chinese Academy of Sciences, Beijing 100101, China

<sup>6</sup>University of Chinese Academy of Sciences, Beijing 100049, China

<sup>7</sup>These authors contributed equally

<sup>8</sup>Lead Contact

\*Correspondence: jllei@tsinghua.edu.cn (J.L.), hongweiwang@tsinghua.edu.cn (H.-W.W.) http://dx.doi.org/10.1016/j.str.2017.08.008

#### **SUMMARY**

Volta phase plate (VPP) is a recently developed transmission electron microscope (TEM) apparatus that can significantly enhance the image contrast of biological samples in cryoelectron microscopy, and therefore provide the possibility to solve structures of relatively small macromolecules at high-resolution. In this work, we performed theoretical analysis and found that using phase plate on objective lens spherical aberration (Cs)-corrected TEM may gain some interesting optical properties, including the over-focus imaging of macromolecules. We subsequently evaluated the imaging strategy of frozenhydrated apo-ferritin with VPP on a Cs-corrected TEM and obtained the structure of apo-ferritin at near-atomic resolution from both under- and overfocused dataset, illustrating the feasibility and new potential of combining VPP with Cs-corrected TEM for high-resolution cryo-EM.

#### INTRODUCTION

The recent technical breakthroughs, such as the invention of the direct electron detector (Faruqi and Henderson, 2007; McMullan et al., 2014) and the implementation of new image-processing algorithms (Brilot et al., 2012; Li et al., 2013; Scheres, 2012), have brought single-particle cryoelectron microscopy (cryo-EM) a stunning capability to determine the structure of macromolecules at atomic or near-atomic resolution (Bai et al., 2015; Cheng et al., 2015; Nogales and Scheres, 2015). As the central instrument of the technology, a modern transmission electron microscope (TEM) has a rather complex electron optics that still has a lot of

space to be further improved. The material science community has witnessed the application of a few new electron optical apparatuses to reveal structures at sub-atomic resolution. It is tempting to explore if cryo-EM technology can benefit from new optical-tuning equipment, including the phase plate and Cs-corrector.

An under-focus data-collection strategy on conventional TEM (CTEM) has been exploited for decades according to the contrast transfer theory that predicts a sine contrast transfer function (CTF) with a small percentage of amplitude contrast for weakphase biological specimens (Frank, 2006). Adding a phase plate at the back-focal plane of the objective lens could modulate the CTF as a cosine function (Danev and Nagayama, 2001; Zernike, 1942). A major advantage of using the phase plate is the strong boost of image contrast because more low-frequency information of the structure is maintained in the image, which is of particular use for biological specimens (Glaeser, 2013). Using the carbon-film-based Zernike phase plate, a few single-particle structures have been obtained using cryo-EM (Dai et al., 2014; Danev et al., 2009; Danev and Nagayama, 2001, 2008; Nagayama, 2008; Taylor et al., 2013). It has also been used in cryoelectron tomography to study cellular structures (Danev et al., 2010; Fukuda and Nagayama, 2012; Guerrero-Ferreira and Wright, 2014; Hosogi et al., 2011; Murata et al., 2010). In 2015, a new type of phase plate using a voltage-charged film, so-called Volta phase plate (VPP), was shown to be able to give high-contrasted images of biological molecules with much less fringes than the Zernike phase plate (Danev et al., 2014). In combination with the direct electron detector, VPP allowed the reconstruction of several protein structures at near-atomic resolution (Chua et al., 2016; Danev and Baumeister, 2016; Khoshouei et al., 2016, 2017; Danev et al., 2017; Liang et al., 2017).

Theoretically there is no information loss in the microscope at all with a perfect phase plate adjusted at  $0.5\pi$  phase shift and a perfect objective lens without spherical aberration. The presence of spherical aberration in the objective lens, however, causes information distortion in the images especially at high



frequency. Such a problem may be overcome by the usage of a Cs-corrector of the objective lens. Compared with results obtained from CTEM (Brown et al., 2016; Passos and Lyumkis, 2015; Shalev-Benami et al., 2016), a Cs-corrector-equipped microscope also has been shown to be able to solve the structure of ribosomes at resolution higher than 3 Å (Fischer et al., 2015, 2016). No attempt has yet been reported to use the combination of phase plate and Cs-corrector for high-resolution cryo-EM, although theoretical analysis and simulation suggests that a combination would maintain more structural information at high spatial frequencies (Evans et al., 2008; Gamm et al., 2008).

In this work, we performed theoretical analysis and noted that the combination of a phase plate and Cs-corrector can generate images suitable for high-resolution structural determination in both the under- and over-focus imaging conditions. Using a VPP on a Cs-corrector-equipped electron microscope, we imaged ice-embedded apo-ferritin molecules under either under- or over-focus imaging conditions. Single-particle analysis of both the under- and over-focused datasets led to reconstructions at  $\sim\!\!3.0~\mbox{\normalfont\AA}$  resolution. The two datasets can also be combined and treated as a single dataset reconstructed at  $3.0~\mbox{\normalfont\AA}$  resolution, illustrating a novel imaging capability for high-resolution cryo-EM by the combination of VPP and Cs-corrector.

#### **RESULTS**

# CTF of Under- and Over-Focus Cryo-EM with Phase Plate and Cs-Corrector

For thin biological specimens in TEM, the weak-phase approximation predicts that the Fourier transform of a TEM image as a multiplication of the Fourier transform of the object's projection and the CTF of the TEM's electron-optic system (Frank, 2006). A simplified form of the CTF can be written as:

CTF(k) = 
$$E(k)\sin\left(Z\pi\lambda k^2 + \frac{1}{2}C_s\lambda^3k^4 - \varphi\right)$$
 (Equation 1)

where k is the spatial frequency in Fourier space;  $\lambda$  is the electron wave length with given acceleration voltage; Z is the defocus value with positive sign for over-focus and negative sign for under-focus imaging condition;  $C_s$  is the spherical aberration of the TEM objective lens;  $\varphi$  is an integrated phase shift combining the amplitude contrast and phase plate effects; and E(k) is the envelope function that modulates the amplitude of CTF. We can calculate the CTFs in respect of the spatial frequency under different imaging scenarios using Equation 1.

For CTEM without phase plate, the  $\varphi$  is a rather small positive value contributed only by the amplitude contrast. When Z is positive (over-focus imaging condition), the CTF starts with a small negative value at zero frequency and crosses the frequency axis rapidly at low frequency (Figure 1A, CTEM blue curve). The precise location of this first zero is correlated to both defocus and the amplitude contrast based on the equation:  $Z\pi\lambda k^2 = \varphi$  (the quadruple term of k is omitted). The precise location of the first CTF zero is quite sensitive to the amplitude contrast  $\varphi$ , which is not easy to determine precisely. Therefore, when Z is positive, the CTF correction in the low-frequency range (1/5 to 1/20 nm in our simulation) could deviate dramatically and

cause an artifact in the reconstruction. In contrast, the underfocus imaging condition (negative Z value) causes the CTF to have a broader bandwidth (from the origin to the first zero) in the low-frequency area (Figure 1A, CTEM red curve), allowing convenient CTF determination and correction, and so has been the norm for cryo-EM imaging for CTEM. The same phenomenon holds for cryo-EM on a Cs-corrected EM (Figure 1A, Cs-corrector only). As predicted by the CTFs, under- and over-focused images show opposite specimen contrasts (Figure 1B).

When applying a phase plate that can generate a phase shift of  $\sim$ 90°, the  $\varphi$  value is close to  $\pi/2$  and the CTF becomes a cosinelike function (Figure 1A, VPP-only and Cs-corrector + VPP). As a result, there is no flip of sign of CTF at the very low frequency irrespective of the Z value's sign, therefore both under- and overfocused imaging conditions lead to the same image contrast (Figure 1C). In principle, for both imaging conditions, the CTF parameters, including Z and  $\varphi$ , can be accurately determined by fitting Equation 1 in the power spectrum of a raw image with the known Cs value. The CTF can subsequently be corrected for image processing with the estimated parameters. We noted that the relatively large Cs value on a normal TEM, i.e., 2.7 mm of Cs on a Titan Krios, causes significant difference of CTF curves for under- and over-focused images, especially at the high-frequency range (Figure 1A, VPP-only). This means that, for phase plate images, a CTF fitting program must take care of the under- or over-focus imaging conditions separately, whereas the sign of the Z value cannot be directly obtained from either the raw image or the power spectrum. As far as we know, the currently available CTF fitting programs do not have the capability to meet such a need. This problem, however, can be eliminated by drastically reducing the Cs value in a TEM equipped with a Cs-corrector. With a very small Cs value ( $\sim$ 0.001 mm), the second term for the sine function in Equation 1 can be neglected. The equation thus becomes:

CTF = 
$$E(k)sin(Z\pi\lambda k^2 - \varphi) \equiv E(k)sin(-Z\pi\lambda k^2 - (\pi - \varphi))$$
 (Equation 2)

If  $\varphi$  is modulated to  $\pi/2$ , the above equation predicts that the same CTF curve would be generated by under- and over-focus imaging conditions with the same absolute defocus value (Figure 1A, Cs-corrector plus VPP). As a matter of fact, as long as the  $\varphi$  is around  $\pi/2$  (not necessarily to be exact), we could treat the over-focused images (positive Z value) in the same way as the under-focused images (negative Z value) except that we need to use a  $\varphi = (\pi - \varphi)$  to perform the CTF fitting. The most current version of CTFFIND 4.15 (Rohou and Grigorieff, 2015) and Gctf-1.06 (Zhang, 2016) programs can be used to search for both Z and  $\varphi$  values for an optimal fitting. The estimated parameters can be directly used for CTF correction in later image-processing steps. In conclusion, the combination of a Cs-corrector and a phase plate allows to image the biological cryo-EM specimens using under- or over-focus imaging conditions and treat the images in exactly the same way.

# Single-Particle Reconstruction of Apo-Ferritin by VPP-Cs-Corrector Coupled Cryo-EM

To test the above theory, we established a procedure (Figure S1; STAR Methods) to collect cryo-EM images of apo-ferritin

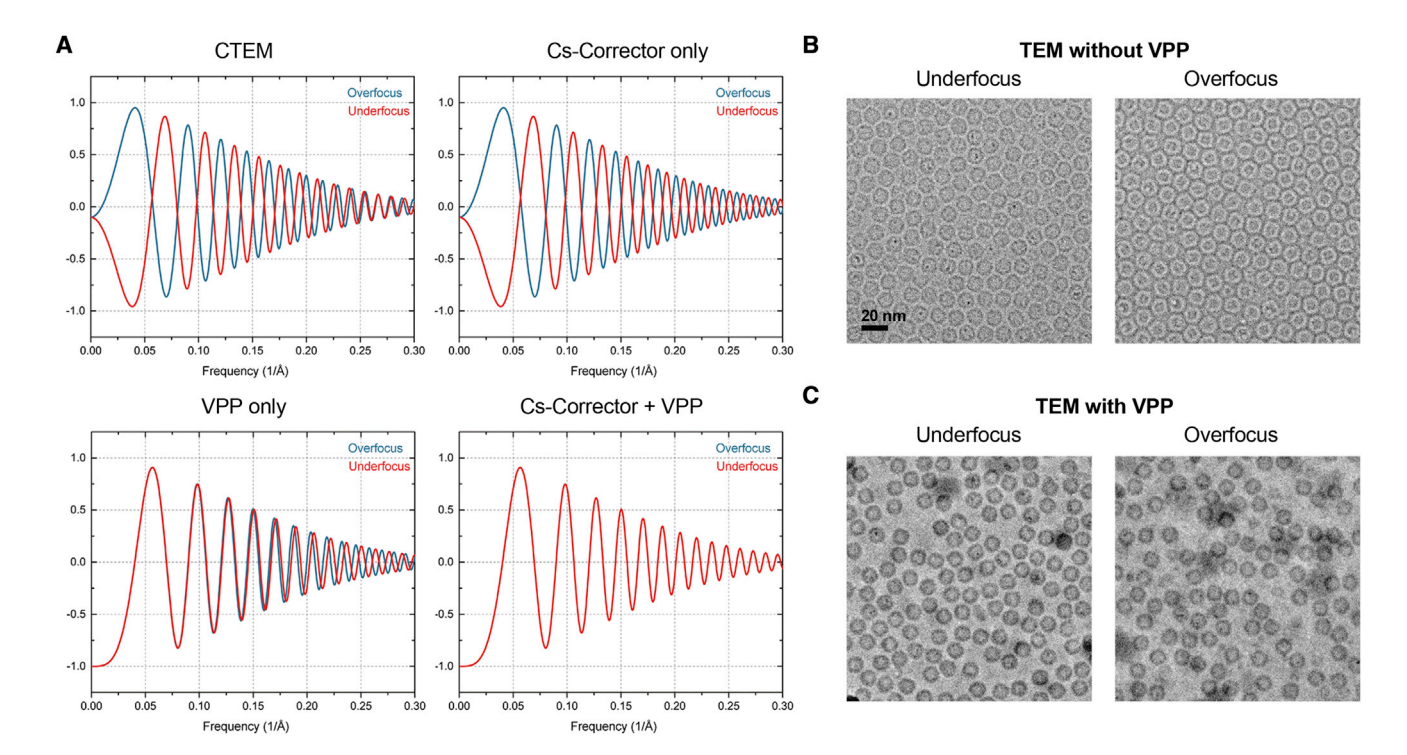


Figure 1. CTF and Cryo-EM Images by VPP-Cs-Corrector Coupled EM

(A) Simulated contrast transfer functions (CTF) in different scenarios. For conventional TEM (CTEM), the spherical aberration (Cs) is 2.7 mm with  $\sim$ 10% amplitude contrast. For Cs-corrected TEM, Cs is set to 0.001 mm (1  $\mu$ m). An ideal VPP which introduces a  $\pi$ /2 phase shift is applied in this simulation. Defocus values of -0.5 and +0.5  $\mu$ m are used for under- or over-focus imaging conditions in all simulations, respectively. We used the same B factor (-30 Å $^{-2}$ ) exponential decay as the simplified envelope function for all simulations.

(B) Micrographs of apo-ferritin particles collected with  $-2.0~\mu m$  under-focus (left) and  $+2.0~\mu m$  over-focus (right) imaging conditions using Cs-corrected TEM. (C) Micrographs of apo-ferritin particles collected at  $-0.6~\mu m$  under-focus with  $0.45~\pi$  phase shift (left) and  $+0.5~\mu m$  over-focus with  $0.58~\pi$  phase shift (right) imaging conditions using Cs-corrected TEM with VPP.

embedded in vitreous ice using the VPP-Cs-corrector coupled crvo-EM. We intentionally collected under- and over-focused datasets of the specimen with the phase shift ranging from  $0.2\pi$  to  $0.8\pi$ . Three datasets were thus generated: (1) an under-focused dataset collected with -0.4 to  $-1.0~\mu m$  defocus, (2) an over-focused dataset collected with 0.4-1.0 μm defocus, and (3) a mixture of under-focused (dataset 1) and over-focused (dataset 2) images. We treated all the three datasets as underfocused images for CTF parameter determination and used all the images regardless of the amount of phase shift within them for single-particle analysis following the standard Relion image-processing strategy (Kimanius et al., 2016). We were able to calculate the 2D class averages that showed fine details of the apo-ferritin in different views indistinguishable among the three datasets (Figure 2A). For all three datasets, we successfully performed 3D classification and refinement and obtained 3D reconstructions of apo-ferritin at 2.9 Å (under-focused dataset; Figure S2A), 3.2 Å (over-focused dataset; Figure S2B), and 3.0 Å (mixed under-/over-focused dataset; Figures 2B and S2C), respectively. The three reconstructions appeared almost exactly the same. The subtle resolution difference seems related to the dataset quality.

We evaluated the cryo-EM reconstructions and compared them with previously solved crystal structures of apo-ferritin. Using the reconstruction from the mixed under-/over-focused dataset as an example, as shown in the local resolution map, the reconstruction as a hollow spherical assembly has the highest resolution in the middle of the shell, reaching to 2.6 Å resolution, and low resolution on the inner and outer surfaces of the assembly (Figure 2B). The quality of the map is good enough to dock a crystal structure of apo-ferritin (PDB: 1FHA; Lawson and Smith, 1991) into the density map with high correlation (0.9078). All the key features of the secondary structural elements and major side chains are clearly visible and match well (Figures 2C-2E and S2D). We then performed a refinement of the docked atomic model against the map, leading to a model with almost no difference from the crystal structure (root-mean-square deviation = 0.08 Å). We noticed that at this resolution of the reconstruction, the major side chains can be easily recognized, especially the aromatic amino acids and positively charged amino acids (Figure S2D). Furthermore, we can distinguish metal ions bound to both the 3- and 4-fold symmetry axis of the complex (Figures 2D and 2E). These proved the capability of VPP-Cs-corrector coupled cryo-EM in resolving high-resolution structures using this novel under- and over-focus imaging method.

In addition, to evaluate the quality of the raw VPP data that contributed to the final high-resolution structure, we investigated the statistics of the particle distribution in the 2.9  $\mathring{\text{A}}$  underfocused reconstruction (Figure 3) and 3.2  $\mathring{\text{A}}$  over-focused

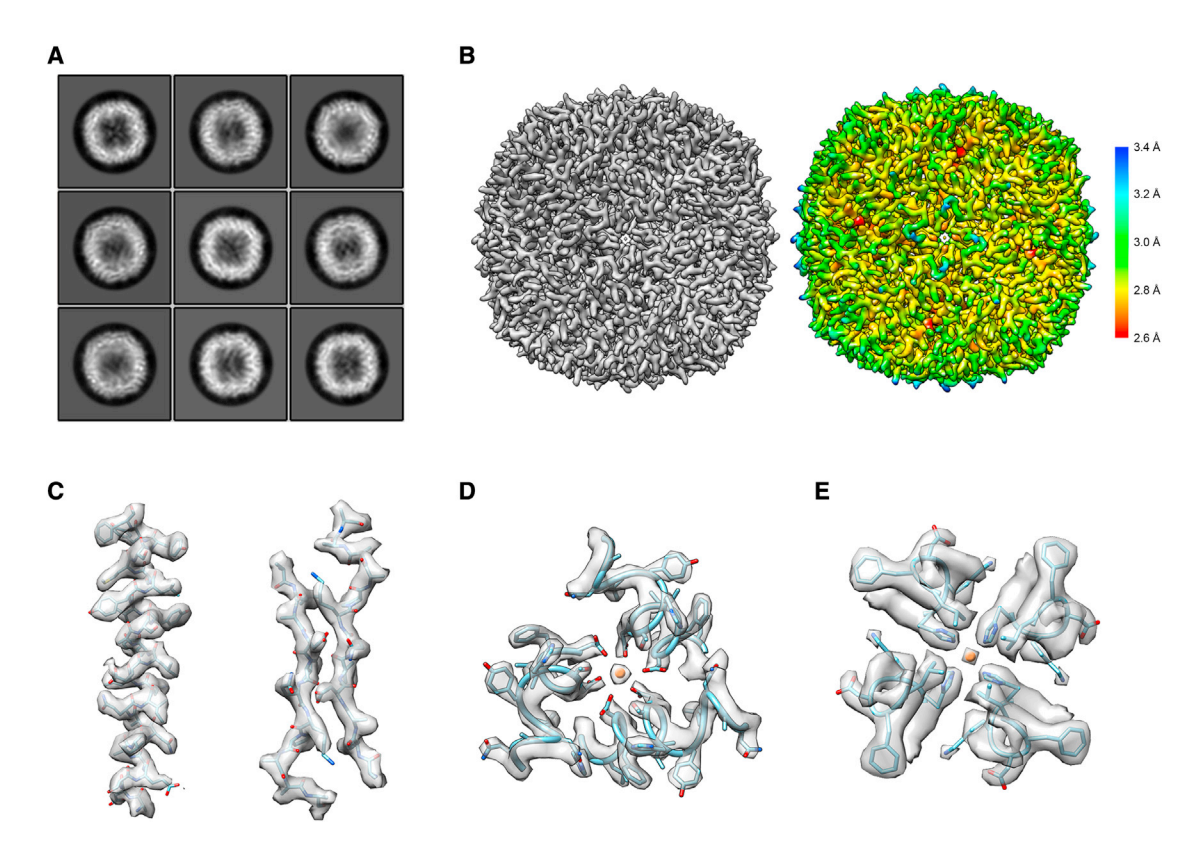


Figure 2. 3D Reconstruction of Mixed Under/Over-Focused Dataset of Apo-Ferritin

- (A) Representative 2D class averages.
- (B) The 3D reconstruction map at 3.0  $\mbox{\normalfont\AA}$  resolution (left) and the local resolution map (right).
- (C) Representative densities of secondary structures:  $\alpha$  helix (left) and  $\beta$  sheet (right).
- (D and E) Ion binding sites of apo-ferritin at its 3-fold (D) and 4-fold (E) symmetric axis.

reconstruction (Figure S4), respectively. As expected, particle images with phase shifts ranging from  $0.4\pi$  to  $0.6\pi$  were the majority using both the absolute number and percentage for the final high-resolution reconstruction, probably because of their high contrast for more accurate alignment (Figures 3A and S4A). The defocus value did not seem to have much effect on the percentage of particles contributing to the final high-resolution reconstruction, except that the images with absolute defocus values lower than 0.2  $\mu m$  contributed less (Figures 3B and S4B). This may reflect the inaccuracy of CTF parameter determination of the near-focus images.

#### **Dose-Dependent Reconstruction of the VPP Dataset**

The signal-to-noise ratio (SNR) of molecule images is a crucial factor for data processing. For CTEM data collection, usually high electron dose or high defocus are used to increase the SNR, especially at a low frequency. But the high electron dose would cause radiation damage of the specimen and the high defocus value would cause inaccuracy of CTF correction at high frequency, both dampening the high-frequency signal. We analyzed the dose-dependence of reconstruction from the VPP dataset. When using CTEM without VPP, in order to clearly see the protein particles, we generally use a total dose 40 to 50 e $^-/\mbox{Å}^2$  and defocus values ranging from -1.0 to  $-2.0~\mu m$  to collect movie stacks. In our case, VPP movie stacks of apo-

ferritin were collected with 25 e $^-/\mbox{Å}^2$  total dose, and absolute defocus values ranging from 0.2 to 0.8  $\mu m$  were enough for image processing (Figures 2, S2, and S3). To evaluate the minimum dose required for high-resolution reconstruction by VPP cryo-EM, we generated summed images with different frame numbers from the original 33-frame movie stacks (Figure 4). In our dataset, we found that a total dose of  $\sim\!15$  e $^-/\mbox{Å}^2$  is sufficient for successful global angular search to reach 3.1  $\mbox{Å}$  resolution (Figure 4A). Following a successful global angular search, local search and refinement can be done with only the first ten frames (a total dose of 7 e $^-/\mbox{Å}^2$ ) to reach high enough resolution to resolve the fine details (Figures 4B and 4C). As a matter of fact, the first ten frames maintained the high-frequency signal better than more frames summed (Figure 4C), demonstrating the accumulation of radiation damage during the exposure process.

#### **DISCUSSION**

Cryo-EM has led structural biology into a new era, in which atomic or near-atomic resolution of macromolecule structures is much easier to be acquired (Bai et al., 2015; Nogales and Scheres, 2015). Research has demonstrated that the application of phase plate or Cs-corrected cryo-EM, respectively, can solve high-resolution structures (Chua et al., 2016; Danev and Baumeister, 2016; Danev et al., 2017; Fischer et al., 2015; Khoshouei

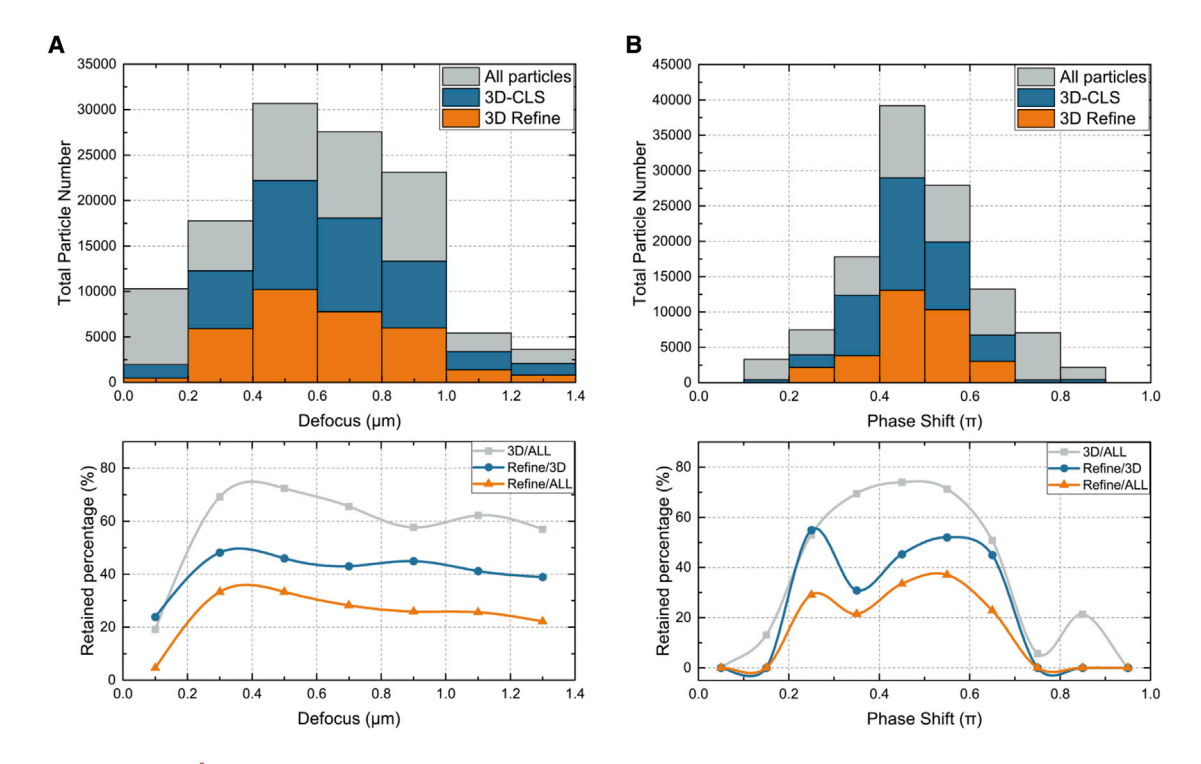


Figure 3. Statistics of 2.9 Å VPP Apo-Ferritin Reconstructions in the Under-Focus Imaging Conditions

(A) Particle distribution in different reconstruction steps according to their defocus values. In the upper panel: All particles (gray), contains all particles automatically picked from the micrographs; 3D-CLS (blue), contains all the particles from the selected good classes after 3D classification in Relion 2.0; 3D Refine (orange), contains the particles used for the best reconstruction. The normalized ratio of retained particles in each step is in the bottom panel, where ALL, 3D, and Refine refer to ALL particles, 3D-CLS, and 3D Refine, respectively.

(B) Particle distribution (upper) and retained percentage (lower) according to their phase shift. The labels are the same as in (A).

et al., 2016). To our knowledge, until now there has been no highresolution structure reported using a combination of the phase plate and Cs-corrector or determined from data collected in over-focus imaging conditions. The case study of apo-ferritin in this work proved in principle, and set a novel data-acquisition strategy, for atomic resolution structure determination using the VPP-Cs-corrector coupled cryo-EM.

The successful reconstruction of apo-ferritin at atomic resolution in over-focus imaging conditions by VPP-Cs-corrector coupled cryo-EM not only proves the feasibility of such a combined optical system, but also introduces some interesting advantages of the system for the cryo-EM community to further investigate. Since the under- and over-focused images are indiscriminate in this system, we could use a data-acquisition strategy by approximately adjusting the specimen to eucentric height, with the objective lens set at eucentric focus, and then automatically collecting data in nearby areas by moving Compustage-XY without further adjusting the objective lens for focusing. This strategy, which keeps the stable optical system in EM during collection, may significantly speed up the data collection and reduce the lens-dependent astigmatism (Yan et al., 2017) during automatic data collection, thus improving the data quality and quantity simultaneously. This system would also change tomography data-collection strategy. Currently, tomography data collection requires the whole tilting series in the under-focus imaging condition for data processing, and thus causes higher defocus values for images collected at high tilt angles. If using the VPP-Cs-corrector coupled system, one may collect tilt series at much lower defocus values, which introduces less phase inversions in high frequency, thus increasing the fidelity of CTF correction for tomography reconstruction. It is also intriguing to find that the minimum total dose used for high-resolution refinement on the VPP-Cs-corrector coupled microscope can be as low as 7 e $^-/\mathring{A}^2$ . This illustrates the power of the new optical systems in cryo-EM of biological specimens, especially for cryoelectron tomography where multiple exposures at very low dose are favored.

Besides the data-acquisition property, the combination of Cs-corrector and VPP also shows a better optical property than when used separately. In a simulation, we found that a relatively large astigmatism could cause the 2D CTF pattern to be distorted from an oval to a hyperbolic shape at high frequency in a system with Cs (Figure 5A). This would be challenging for both CTF estimation and correction, especially for near-focus images. Such a behavior caused by astigmatism and Cs are more devastating for VPP images, because, as a matter of practical fact, VPP may introduce extra astigmatism to final images. In a system with a Cs-corrector that reduces the Cs value, the hyperbolic shape disappears from the astigmatic CTF pattern, and therefore high-frequency signals are well retained (Figure 5B).

The optical system of a Cs-corrector coupled with VPP needs a stable alignment of the Cs-corrector and VPP during the image acquisition. We therefore tried to minimize the adjustment of the

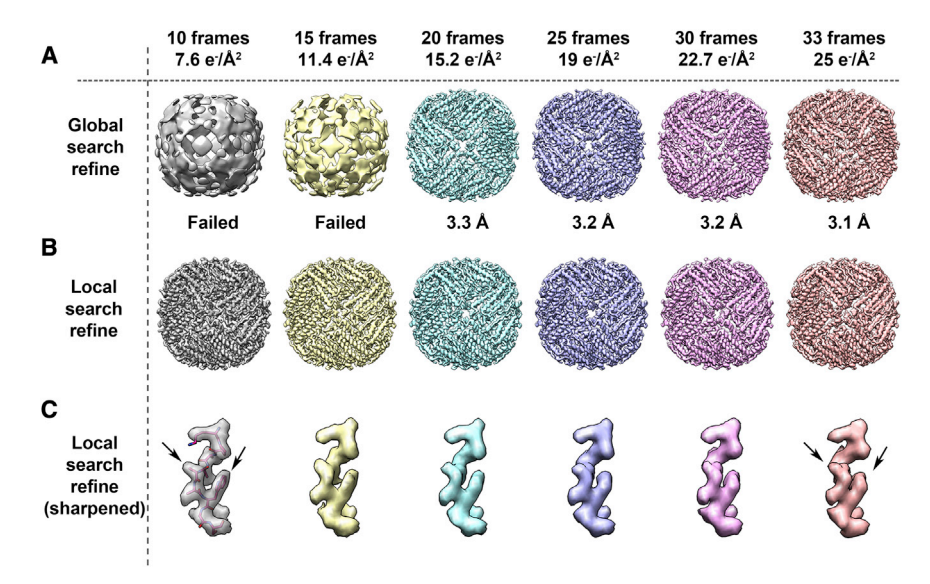


#### Figure 4. Dose-Dependent Reconstructions

(A) The global search reconstructions resulted from different frame combinations. The first 10, 15, 20. 25, and 30 frames (7.6, 11.4, 15.2, 19, and 22.7  $e^-/\mbox{Å}^2$  in total dose), and full 33 frames (25 e-/Å2 in total dose) are motion-corrected, summed, and refined using global angular search in Relion 2.0 individually with the same setting (7.5° initial angular sampling with 5 pixels initial offset range). Unsharpened maps (without post-process) are shown here with the reported resolution labeled underneath. "Failed" means that the reconstruction did not reach correct convergence.

- (B) The local search refinement results from different frame combinations. The angular and offset information from the best reconstruction are applied for a local search from 1.8° with 3 pixels offset range. All the reconstructions reached to very similar resolutions
- (C) Representative region (loop with residues 87-95) from the sharpened maps of apo-ferritin (B factor -150 Å-2) from each local search refinement. The corresponding atomic model was fitted in the first map. Black arrows indicate the density deteriorated with more dose accumulation.

objective lens current (defocus value) and the retraction and insertion operation of the VPP aperture. Instead, we maintained the system at eucentric focus and adjusted the defocus by directly changing the Z height of the specimen with Compustage to maintain the Cs-corrector at its best performance position at the preset eucentric focus. We used a modified version of the AutoEMation (Lei and Frank, 2005) software to meet our needs on the VPP-Cs-corrector coupled Titan Krios instrument for a semi-automatic data collection. This software can be further improved to become fully automatic in the future, especially given that the focusing step could be largely eliminated due to the system's novel properties. In the future microscope, when the next generation of Cs-correctors becomes more stable and is able to correct off-axis coma, and the phase plate becomes more robust, the combination of phase plate and Cs-corrector may become a powerful tool for high-resolution cryo-EM.

In conclusion, with this work we have demonstrated the feasibility of getting high-resolution structures in over-focus imaging condition with the combination of a VPP and a Cs-corrector, potentiating the use of this method as a new approach for cryo-EM data acquisition. Further experiments with smaller or low-symmetry samples should be performed in the future and the advantages introduced by this novel system should be further explored for electron tomography.

#### **STAR**\*METHODS

Detailed methods are provided in the online version of this paper and include the following:

- KEY RESOURCES TABLE
- CONTACT FOR REAGENT AND RESOURCE SHARING
- METHOD DETAILS
  - O Assessment of Volta Phase Plate
  - Protein Sample Preparation
  - Cryo-EM Sample Preparation

- Data Collection
- Data Processing
- O Dose-Dependent Reconstruction
- Model Fitting and Refinement
- QUANTIFICATION AND STATISTICAL ANALYSIS
  - Particle Distribution Analysis
- DATA AND SOFTWARE AVAILABILITY

#### **SUPPLEMENTAL INFORMATION**

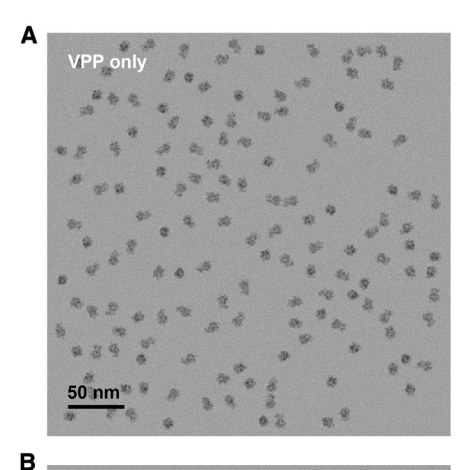
Supplemental Information includes five figures and one data file and can be found with this article online at http://dx.doi.org/10.1016/i.str.2017.08.008.

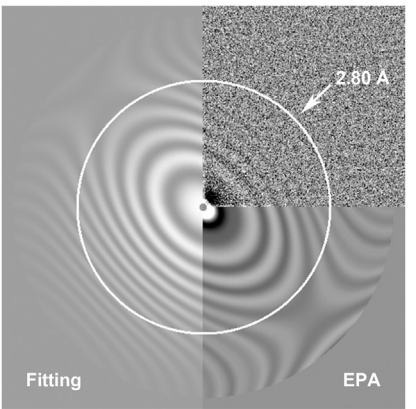
## **AUTHOR CONTRIBUTIONS**

X.F., L.Z., J.L., and H.-W.W. conceived the experiments and wrote/corrected the manuscript. X.F. and L.Z. performed the cryo-EM sample preparation, data collection, and processing. J.Z. and H.-L.P. prepared graphene grids. C.L. aided in grid preparation. K.F. and X.Y. provided apo-ferritin sample. J.L. aided in hardware setup and data collection.

#### **ACKNOWLEDGMENTS**

Our sincere thanks to R.M. Glaser (UC-Berkeley) and R. Danev (Max-Plank Institute of Biochemistry) for their helpful advice in setting up the VPP. We thank Y.C. Deng (FEI Company) and K. Zhang (MRC-LMB) for the helpful discussions of CTF fitting and correction, Q. Zhou (Tsinghua University) for image simulation, X.M. Li and T. Yang at the Tsinghua University Branch of the National Protein Science Facility (Beijing) for their technical support on the Cryo-EM and High-Performance Computation platforms, F. Sun and X.J. Huang (Institute of Biophysics, CAS) for their help with the apo-ferritin sample. This work was supported by grant 2016YFA0501100 (to H.-W.W.) from the Ministry of Science and Technology of China, grant Z161100000116034 (to H.-W.W.) from the Beijing Municipal Science & Technology Commission. K. Fan is supported by the Young Elite Scientist Sponsorship Program by CAST, Beijing Natural Science Foundation (no. 5164037), China Postdoctoral Science Foundation (no. 2015M570158), and the China Postdoctoral Science Special Foundation (no. 2016T90143).





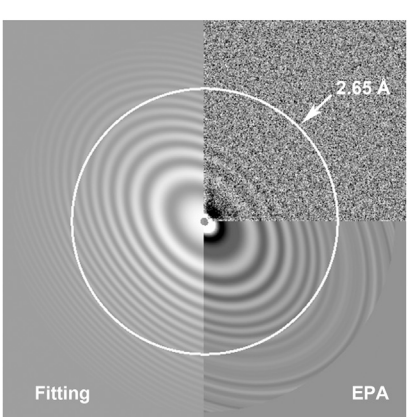


Figure 5. Simulations on the Anti-astigmatism Ability of the Cs-Corrector

(A and B) Simulated VPP images (left) and their CTF estimation results using Gctf program (right). Cs value is the only difference between the two simulated images. The common parameters are: defocus U 0.4  $\mu$ m, defocus V 0.2  $\mu$ m, astigmatism angle 45°, and phase shift  $\pi/2$ . For VPP-only condition (A), the Cs is 2.7 mm. For Cs-corrected TEM (B), the value is 0.001 mm. For CTF estimation in Gctf, the upper right corner is the power spectrum of real space image, the lower right corner is the equi-phase average result and the left half is the theoretical CTF fitting result. The white circles indicate the maximum resolution of the signal estimated by Gctf from images.

Received: June 6, 2017 Revised: July 25, 2017 Accepted: August 15, 2017 Published: September 21, 2017

#### REFERENCES

Bai, X.-C., McMullan, G., and Scheres, S.H. (2015). How cryo-EM is revolutionizing structural biology. Trends Biochem. Sci. 40, 49-57.

Brilot, A.F., Chen, J.Z., Cheng, A., Pan, J., Harrison, S.C., Potter, C.S., Carragher, B., Henderson, R., and Grigorieff, N. (2012). Beam-induced motion of vitrified specimen on holey carbon film. J. Struct. Biol. 177, 630-637.

Brown, A., Fernández, I.S., Gordiyenko, Y., and Ramakrishnan, V. (2016). Ribosome-dependent activation of stringent control. Nature 534, 277–280.

Cheng, Y., Grigorieff, N., Penczek, P.A., and Walz, T. (2015). A primer to singleparticle cryo-electron microscopy. Cell 161, 438-449.

Chua, E.Y., Vogirala, V.K., Inian, O., Wong, A.S., Nordenskiöld, L., Plitzko, J.M., Danev, R., and Sandin, S. (2016). 3.9 Å structure of the nucleosome core particle determined by phase-plate cryo-EM. Nucleic Acids Res. 44,

Dai, W., Fu, C., Khant, H.A., Ludtke, S.J., Schmid, M.F., and Chiu, W. (2014). Zernike phase-contrast electron cryotomography applied to marine cyanobacteria infected with cyanophages. Nat. Protoc. 9, 2630-2642.

Danev, R., and Baumeister, W. (2016). Cryo-EM single particle analysis with the Volta phase plate. Elife 5, e13046.

Danev, R., Glaeser, R.M., and Nagayama, K. (2009). Practical factors affecting the performance of a thin-film phase plate for transmission electron microscopy. Ultramicroscopy 109, 312-325.

Daney, R., Kanamaru, S., Marko, M., and Nagayama, K. (2010). Zernike phase contrast cryo-electron tomography. J. Struct. Biol. 171, 174-181.

Danev, R., Buijsse, B., Khoshouei, M., Plitzko, J.M., and Baumeister, W. (2014). Volta potential phase plate for in-focus phase contrast transmission electron microscopy. Proc. Natl. Acad. Sci. USA 111, 15635-15640.

Daney, R., Tegunov, D., and Baumeister, W. (2017). Using the Volta phase plate with defocus for cryo-EM single particle analysis. Elife 6, e23006.

Danev, R., and Nagayama, K. (2001). Transmission electron microscopy with Zernike phase plate. Ultramicroscopy 88, 243.

Danev, R., and Nagayama, K. (2008). Single particle analysis based on Zernike phase contrast transmission electron microscopy. J. Struct. Biol. 161,

Emsley, P., Lohkamp, B., Scott, W.G., and Cowtan, K. (2010). Features and development of Coot. Acta Crystallogr. D Biol. Crystallogr. 66, 486-501.

Evans, J.E., Hetherington, C., Kirkland, A., Chang, L.-Y., Stahlberg, H., and Browning, N. (2008). Low-dose aberration corrected cryo-electron microscopy of organic specimens. Ultramicroscopy 108, 1636-1644.

Fan, K., Cao, C., Pan, Y., Lu, D., Yang, D., Feng, J., Song, L., Liang, M., and Yan, X. (2012). Magnetoferritin nanoparticles for targeting and visualizing tumour tissues. Nat. Nanotechnol. 7, 459-464.

Faruqi, A., and Henderson, R. (2007). Electronic detectors for electron microscopy. Curr. Opin. Struct. Biol. 17, 549-555.

Fischer, N., Neumann, P., Konevega, A.L., Bock, L.V., Ficner, R., Rodnina, M.V., and Stark, H. (2015). Structure of the E. coli ribosome-EF-Tu complex at <3 Å resolution by Cs-corrected cryo-EM. Nature 520, 567-570.

Fischer, N., Neumann, P., Bock, L.V., Maracci, C., Wang, Z., Paleskava, A., Konevega, A.L., Schröder, G.F., Grubmüller, H., and Ficner, R. (2016). The pathway to GTPase activation of elongation factor SelB on the ribosome. Nature 540, 80-85.

Frank, J. (2006). Three-Dimensional Electron Microscopy of Macromolecular Assemblies: Visualization of Biological Molecules in Their Native State (Oxford University Press).

Fukuda, Y., and Nagayama, K. (2012). Zernike phase contrast cryo-electron tomography of whole mounted frozen cells. J. Struct. Biol. 177, 484-489.

Gamm, B., Schultheiß, K., Gerthsen, D., and Schröder, R.R. (2008). Effect of a physical phase plate on contrast transfer in an aberration-corrected transmission electron microscope. Ultramicroscopy 108, 878-884.

Glaeser, R.M. (2013). Invited review article: methods for imaging weak-phase objects in electron microscopy. Rev. Sci. Instrum. 84, 312.

Guerrero-Ferreira, R.C., and Wright, E.R. (2014). Zernike phase contrast cryoelectron tomography of whole bacterial cells. J. Struct. Biol. 185, 129-133.

Hosogi, N., Shigematsu, H., Terashima, H., Homma, M., and Nagavama, K. (2011). Zernike phase contrast cryo-electron tomography of sodium-driven flagellar hook-basal bodies from Vibrio alginolyticus. J. Struct. Biol. 173, 67-76.

Khoshouei, M., Radjainia, M., Phillips, A.J., Gerrard, J.A., Mitra, A.K., Plitzko, J.M., Baumeister, W., and Danev, R. (2016). Volta phase plate cryo-EM of the small protein complex Prx3. Nat. Commun. 7, 10534.

Khoshouei, M., Radjainia, M., Baumeister, W., and Danev, R. (2017). Cryo-EM structure of haemoglobin at 3.2 Å determined with the Volta phase plate. Nat. Commun. 8, 16099.

Kimanius, D., Forsberg, B.O., Scheres, S.H., and Lindahl, E. (2016). Accelerated cryo-EM structure determination with parallelisation using GPUs in RELION-2. Elife 5, e18722.

Lawson, D.M., and Smith, J.M. (1991). Solving the structure of human H ferritin by genetically engineering intermolecular crystal contacts. Nature 349, 541.

Lei, J., and Frank, J. (2005). Automated acquisition of cryo-electron micrographs for single particle reconstruction on an FEI Tecnai electron microscope. J. Struct. Biol. 150, 69-80.

Li, X., Mooney, P., Zheng, S., Booth, C.R., Braunfeld, M.B., Gubbens, S., Agard, D.A., and Cheng, Y. (2013). Electron counting and beam-induced motion correction enable near-atomic-resolution single-particle cryo-EM. Nat. Methods 10, 584.

Liang, M., Fan, K., Zhou, M., Duan, D., Zheng, J., Yang, D., Feng, J., and Yan, X. (2014). H-ferritin - nanocaged doxorubicin nanoparticles specifically target and kill tumors with a single-dose injection. Proc. Natl. Acad. Sci. USA 111, 14900-14905.

Liang, Y.-L., Khoshouei, M., Radjainia, M., Zhang, Y., Glukhova, A., Tarrasch, J., Thal, D.M., Furness, S.G., Christopoulos, G., and Coudrat, T. (2017), Phaseplate cryo-EM structure of a class B GPCR-G-protein complex. Nature 546, 118-123.

McMullan, G., Faruqi, A., Clare, D., and Henderson, R. (2014). Comparison of optimal performance at 300keV of three direct electron detectors for use in low dose electron microscopy. Ultramicroscopy 147, 156-163.

Murata, K., Liu, X., Danev, R., Jakana, J., Schmid, M.F., King, J., Nagayama, K., and Chiu, W. (2010). Zernike phase contrast cryo-electron microscopy and tomography for structure determination at nanometer and subnanometer resolutions. Structure 18, 903-912.

Nagayama, K. (2008). Development of phase plates for electron microscopes and their biological application. Eur. Biophys. J. 37, 345.

Nogales, E., and Scheres, S.H. (2015), Crvo-EM; a unique tool for the visualization of macromolecular complexity. Mol. Cell 58, 677-689.

Passos, D.O., and Lyumkis, D. (2015). Single-particle cryoEM analysis at nearatomic resolution from several thousand asymmetric subunits. J. Struct. Biol. 192, 235-244.

Pettersen, E.F., Goddard, T.D., Huang, C.C., Couch, G.S., Greenblatt, D.M., Meng, E.C., and Ferrin, T.E. (2004). UCSF Chimera — a visualization system for exploratory research and analysis. J. Comput. Chem. 25, 1605-1612.

Rohou, A., and Grigorieff, N. (2015). CTFFIND4: fast and accurate defocus estimation from electron micrographs. J. Struct. Biol. 192, 216-221.

Scheres, S.H.W. (2012). RELION: implementation of a Bayesian approach to cryo-EM structure determination. J. Struct. Biol. 180, 519-530.

Shalev-Benami, M., Zhang, Y., Matzov, D., Halfon, Y., Zackay, A., Rozenberg, H., Zimmerman, E., Bashan, A., Jaffe, C.L., and Yonath, A. (2016). 2.8-Å cryo-EM structure of the large ribosomal subunit from the eukaryotic parasite Leishmania. Cell Rep. 16, 288-294.

Tang, G., Peng, L., Baldwin, P.R., Mann, D.S., Jiang, W., Rees, I., and Ludtke, S.J. (2007). EMAN2: an extensible image processing suite for electron microscopy. J. Struct. Biol. 157, 38-46.

Taylor, D.W., Ma, E., Shigematsu, H., Cianfrocco, M.A., Noland, C.L., Nagayama, K., Nogales, E., Doudna, J.A., and Wang, H.-W. (2013). Substrate-specific structural rearrangements of human Dicer. Nat. Struct. Mol. Biol. 20, 662-670.

Yan, R., Li, K., and Jiang, W. (2017). Defocus and magnification dependent variation of TEM image astigmatism. bioRxiv, 138255, http://dx.doi.org/10. 1101/138255.

Zernike, F. (1942). Phase contrast, a new method for the microscopic observation of transparent objects part II \*. Physica 9, 974-980.

Zhang, J., Lin, L., Sun, L., Huang, Y., Koh, A.L., Dang, W., Yin, J., Wang, M., Tan, C., and Li, T. (2017). Single crystals: clean transfer of large graphene single crystals for high-intactness suspended membranes and liquid cells. Adv. Mater. 29, http://dx.doi.org/10.1002/adma.201770188.

Zhang, K. (2016). Gctf: real-time CTF determination and correction. J. Struct. Biol. 193, 1-12.

Zheng, S.Q., Palovcak, E., Armache, J.-P., Verba, K.A., Cheng, Y., and Agard, D.A. (2017). MotionCor2: anisotropic correction of beam-induced motion for improved cryo-electron microscopy. Nat. Methods 14, 331-332.

# **STAR**\***METHODS**

#### **KEY RESOURCES TABLE**

REAGENT or RESOURCE	SOURCE	IDENTIFIER
Bacterial and Virus Strains		
Escherichia coli: BL21(DE3) strain	TransGen Biotech	CD601-01
Chemicals, Peptides, and Recombinant Proteins		
Human heavy-chain apo-ferritin	(Fan et al., 2012)	N/A
Graphene	(Zhang et al., 2017)	N/A
isopropyl-β-D-thiogalactoside	Sigma-Aldrich	I6758
DNAse	Sigma-Aldrich	D5025
RNAse	Sigma-Aldrich	R4642
Critical Commercial Assays		
BCA protein assay kit	Pierce	23225
Deposited Data		
Under-focused apoferritin structure	This paper	EMData Bank: EMD-6800
Over-focused apoferritin structure	This paper	EMData Bank: EMD-6801
Mixed under-/over-focused apoferritin structure	This paper	EMData Bank: EMD-6802
Recombinant DNA		
HFn-pET-30a(+)	(Fan et al., 2012)	N/A
Software and Algorithms		
MotionCor	(Li et al., 2013)	http://cryoem.ucsf.edu/software/ driftcorr.html
MotionCor2	(Zheng et al., 2017)	http://msg.ucsf.edu/em/software/ motioncor2.html
RELION2	(Kimanius et al., 2016)	http://www2.mrc-lmb.cam.ac.uk/relion/index.php/Main_Page
CTFFIND4	(Rohou and Grigorieff, 2015)	http://grigoriefflab.janelia.org/ctffind4
GCTF	(Zhang, 2016)	http://www.mrc-lmb.cam.ac.uk/ kzhang/Gctf/
AutoEMation	(Lei and Frank, 2005)	N/A
EMAN2	(Tang et al., 2007)	http://blake.bcm.edu/EMAN2/
Coot	(Emsley et al., 2010)	http://www2.mrc-lmb.cam.ac.uk/Personal/pemsley/coot/
UCSF Chimera	(Pettersen et al., 2004)	http://www.cgl.ucsf.edu/chimera/
Other		
EM-grid (Quantifoil, R1.2/1.3)	Quantifoil Micro Tools GmbH, Großlöbichau, Germany	http://www.quantifoil.com/index.php? name=circular
Vitrobot	FEI Company, Netherlands	https://www.fei.com/products/vitrobot/
Sepharose 6 PG XK 16/70	GE Healthcare	90100042
Q-Sepharose Fast Flow	GE Healthcare	17051001

# **CONTACT FOR REAGENT AND RESOURCE SHARING**

Further information and requests for reagents should be directed to and will be fulfilled by the Lead Contact, Hong-Wei Wang (hongweiwang@tsinghua.edu.cn).

## **METHOD DETAILS**

# **Assessment of Volta Phase Plate**

Phase plate behaviors in different conditions were evaluated by measuring phase shift (PS) curves (Figure S5, blue) on amorphous carbon. Quantifoil R1.2/1.3 grids were loaded to a Cs-corrector Titan Krios (FEI Company) that is equipped with a VPP (FEI

Company). After a rough direct alignment process in the micro-probe mode, the nano-probe mode was used for fine alignment of the VPP at the back-focal plane of the objective lens. We used C2 aperture with 50  $\mu$ m, spot size 5 and  $\sim$ 1.1  $\mu$ m illumination area to align the VPP and exactly the same setting for exposure. Exposure dose was measured and proper exposure time was calculated from the AutoEMation (Lei and Frank, 2005) software to make the accumulated dose for each micrograph at about 0.5 nC. Amorphous carbon areas with good quality were selected and set to certain defocus for exposure. For each dataset, a micrograph without VPP was taken first. After VPP was inserted, a series of micrographs (usually 50-100 micrographs) were automatically and continuously collected using the AutoEMation software without changing defocus values. The PS and defocus value of each micrograph were estimated using the CTFFIND 4.15 package (Rohou and Grigorieff, 2015) and Gctf-1.06 (Zhang, 2016). The PS curves were drawn by Origin 8.5 (OriginLab). We chose the VPP with the best behavior from the above measurement for cryo-EM data collection.

#### **Protein Sample Preparation**

Purification of the human heavy-chain ferritin (HFn) was performed as described earlier (Fan et al., 2012; Liang et al., 2014). To produce HFn protein, the expression vector HFn-pET-30a(+) from previous work (Fan et al., 2012) was transformed into *E. coli BL21(DE3)* (TransGen Biotech) according to the manufacturer's instructions. The transformed *E. coli* cells were grown overnight in LB medium with 50 mg/L kanamycin. Then, HFn protein production was induced by isopropyl-β-D-thiogalactoside (IPTG, 0.75 mM, Sigma-Aldrich), and cells were incubated for an additional 4 h. The HFn protein was expressed in *E. coli* where it self-assembled into the 24 subunit apo-ferrintin nano-cage. After the incubation, *E. coli* cells were harvested by centrifugation at 4,500 g for 45 min and the pellets were re-suspended in TBS buffer (20 mM Tris, 150 mM NaCl, pH 8.0). The re-suspended E. coli cells was sonicated on ice and centrifuged at 15,000 g for 30 min. The supernatant was heated at 72°C for 10 min to denature and precipitate most *E. coli* proteins. After centrifugation, the HFn proteins in supernatant were precipitated by ammonium sulfate (520 g/L). The precipitate was collected by centrifugation at 22,000 g for 45 min, and then dissolved in PBS buffer (50 mM NaH2PO4, 150 mM NaCl, pH 7.4). After dialyzing out the ammonium sulfate, DNAse and RNAse (Sigma-Aldrich) were added to final concentration of 60 and 100 μg/mL, respectively, and incubated for 30 min at room temperature. Finally, HFn protein was purified by size exclusion chromatography on a Sepharose 6 PG XK 16/70 column (GE Healthcare) followed by ion-exchange chromatography on Q-Sepharose Fast Flow (GE Healthcare). The concentration of HFn was determined in triplicate by the BCA protein assay kit (Pierce) using bovine serum albumin as the standard.

#### **Cryo-EM Sample Preparation**

Cryo-EM samples were made by Vitrobot (FEI Company). 300 mesh Quantifoil Au R1.2/1.3 grid coated with a graphene film (Zhang et al., 2017) was firstly glow discharged with air. 3 µl purified human apo-ferritin sample (1 mg/ml) was added to the glow discharged grid in Vitrobot Mark IV and waited for 30s. A blot force of -1 and blot time of 1s were applied to blot the grid after waiting. After removing most of the liquid, the grid was plugged into liquid ethane pre-cooled by liquid nitrogen. Cryo-EM samples were stored in liquid nitrogen until examination and data collection on the Cs-corrector Titan Krios microscope equipped with VPP.

#### **Data Collection**

After cryo-EM specimens were loaded into the Titan Krios microscope, areas with visible features (e.g. ice contamination) were used for basic direct alignment and low dose module alignment (set search mode imageshift and focus mode off-axis shift) in micro-probe mode. Amorphous carbon areas were used to finely adjust eucentric-height and eucentric-focus of the specimen. The Cs-corrector (FEI Company) was adjusted at 195,000x magnification using Falcon II camera and FEI image-corrector program to set the Cs value within 5  $\mu$ m. The exposure mode in low dose module was set to nano-probe mode for VPP alignment and data collection. After a VPP was well aligned, we retracted the VPP aperture and used the AutoEMation software to get the atlas of the Quantifoil grid's square in the search mode of low dose module. Individual holes targeted for data collection were identified by AutoEMation automatically. We manually grouped holes in each 10  $\mu$ m radius area and automatically measured and recorded the in-focus height at eucentric focus in the middle of the area using a carbon region. After all the on-focus heights and the coordinates of the targeted holes were recorded, the VPP aperture was inserted back into the beam path. A carbon area on the specimen was continuously illuminated for about 30-60s (according to the phase shfit curve and the exposure dose) to build a  $0.3\pi$  initial PS on the VPP. Micrographs of the apo-ferritin in the targeted holes were then automatically collected using the AutoEMation software at a nominal magnification of 75,000 on a Falcon II camera with movie mode for 33 frames in a 4 sec exposure time, corresponding to a total dose of 25 e-/Ų and pixel size 0.88 Å at the specimen level. Because the in-focus heights in eucentric focus were pre-recorded, the focus step in low dose were skipped. The defocus of each exposure was set in AutoEMation automatically by adjusting the Z-height at eucentric focus.

#### **Data Processing**

Raw frames of Falcon II camera were integrated to a stack with MRC format by a local-written program Raw2MRC. MotionCorr (Li et al., 2013) was firstly used to do full-frame alignment and generated corrected movie stacks for initial examination and screening of good specimen regions. The corrected movie stacks of good specimen were further processed by MotionCorr2 (Zheng et al., 2017) for a 7x7 patches drift correction with dose weighting (-PixSize 0.88 -kV 300 -lter 30 -Patch 7 7 -FmDose 0.75 -Bft 150). The non-dose-weighted images were used for CTF estimation by CTFFIND 4.15 (Rohou and Grigorieff, 2015) and Gctf-1.06 (Zhang, 2016). This allowed for determination of both the absolute defocus value and the phase shift. The estimated phase shift curve tendency of images taken with the same VPP area can help determine whether the images are over-focused or under-focused based

on Equation 2 (Figure S5, orange curve for over-focused images). The CTF fitting of each micrograph was examined and screened by checking the Thon ring fitting accuracy. Only those micrographs with good fitting beyond 4.5 Å resolution were used for further processing. The dose-weighted images were used for particle picking and reconstruction. For under-focused dataset, 118,524 particles were semi-automatically picked by e2boxer.py (Tang et al., 2007) from 375 micrographs. For over-focused dataset, 142,624 were semi-automatically picked by e2boxer.py from 544 micrographs. Multiple rounds of 2D or 3D classification were performed in Relion 2.0 (Kimanius et al., 2016) to screen the best particles producing the two 3D reconstructions of apo-ferritin at about 2.9 Angstrom resolution (under-focused dataset, 32,585 particles) and 3.2 Angstrom resolution (over-focused dataset, 51,722 particles) based on the gold-standard FSC criterion. The mixed dataset (121,653 particles) were from a combined dataset including particles after the first round of 3D classification from under- and over-focused datasets.

#### **Dose-Dependent Reconstruction**

For dose-dependent reconstruction, we generated "partial-dose" stacks from each corrected 33-frame movie stack with different combination of frame numbers and performed patch-drift correction of each frame-truncated stack independently using MotionCor2 with the "-Trunc" option and the same values for other parameters as described in the previous section. Particles were re-extracted from the new partial-dose motion-corrected images using their corresponding star files in Relion 2.0. We used 7.5-degree initial angular sampling with 5 pixels initial offset range for the global search refinement in Relion 2.0 on each partial-dose dataset. For local refinement of each partial-dose dataset, we used the angular information from the whole-frame global refinement as initial values and 1.8-degree initial angular sampling with 3 pixels initial offset range in Relion 2.0.

#### **Model Fitting and Refinement**

The atomic model of human apo-ferritin (1FHA) was fit into the EM density map as a rigid body in UCSF-Chimera (Pettersen et al., 2004). The crystal structure fits quite well with our high-resolution EM density map. However, in the original crystal structure (1FHA) some side chains of the amino acids were missing. In our high-resolution reconstruction, we complement all the missing side chains in Coot (Emsley et al., 2010), including Q14, R22, K49, K53, E61, E64, F81, Q83, D89, C90, D91, D92, E94, H105, K119, E140, K157, E170. Among these, most side chains are clearly visible, especially aromatic and positively charged amino acids.

#### **QUANTIFICATION AND STATISTICAL ANALYSIS**

### **Particle Distribution Analysis**

Particle distributions (Figures 3 and S4) within certain defocus/phaseshift range were counted separately by Excel (Microsoft Company) using the star file, which included all particle information, generated by Relion. The retained percentages were calculated from the counted particle numbers by Excel. Figures 3 and S4 were prepared in Origin using calculated results from Excel.

#### **DATA AND SOFTWARE AVAILABILITY**

All software used are reported in Method Details and indicated in the Key Resources Table. The accession number for the EM maps of apo-ferritin reported in this paper are EMD: 6800, 6801 and 6802.